NACA

RESEARCH MEMORANDUM

WIND-TUNNEL INVESTIGATION OF THE DAMPING IN ROLL OF THE DOUGLAS D-558-II RESEARCH AIRPLANE AND ITS COMPONENTS AT SUPERSONIC SPEEDS

By Russell W. McDearmon

Langley Aeronautical Laboratory
Langley Field, Va.

NATIONAL ADVISORY COMMITTEE
FOR AERONAUTICS

WASHINGTON

September 7, 1956

NATIONAL ADVISORY COMMITTEE FOR AERONAUTICS

RESEARCH MEMORANDUM

WIND-TUNNEL INVESTIGATION OF THE DAMPING IN ROLL OF THE DOUGLAS D-558-II RESEARCH AIRPLANE AND ITS COMPONENTS AT SUPERSONIC SPEEDS

By Russell W. McDearmon

SUMMARY

Experimental values of the damping in roll at zero angle of attack of the Douglas D-558-II research airplane and its components have been obtained at Mach numbers of 1.62, 1.94, 2.22, 2.41, and 2.62.

The general levels and trends of the variations of the damping in roll with Mach number for the complete model and its components were of the order predicted by theory. For some configurations, the contributions of the tail panels to the damping in roll were partially nullified by the flow field behind the wing and other interference effects. Large effects of Reynolds number, boundary layer, and wing-incidence angle on the damping in roll were obtained. The canopy had little effect on the damping in roll.

INTRODUCTION

Dynamic stability problems have been encountered in flight tests of the Douglas D-558-II research airplane at supersonic speeds. In order to obtain some experimental information to provide insight into these problems, a general program of investigations has been undertaken in the Langley 9-inch supersonic tunnel of some of the dynamic and static stability characteristics of the Douglas D-558-II.

The primary purpose of the present investigation was to determine the variation of the damping in roll C_{l_p} of the Douglas D-558-II research airplane with Mach number and to show the contributions of the airplane components to C_{l_p}, at zero angle of attack. In addition, some effects of Reynolds number, boundary layer, wing-incidence angle, and the canopy were determined, and comparisons were made with some theoretical predictions.

The Mach number range of the investigation was from 1.62 to 2.62. The test Reynolds number range was from 0.33×10^6 to 1.52×10^6, based on the mean aerodynamic chord of the wing. The models were tested in the clean condition and with transition strips on the components. With transition strips on the components, boundary-layer conditions encountered at higher Reynolds numbers were probably simulated.

SYMBOLS

b	wing span, ft
C_l	rolling-moment coefficient, M_X/qSb
C_{l_p}	damping-in-roll derivative, $\frac{\partial C_l}{\partial \frac{pb}{2V}}$
i_w	angle of incidence of wing, deg
M_X	rolling moment about longitudinal stability axis
M	free-steam Mach number
p	rolling angular velocity, radians/sec
$pb/2V$	wing-tip helix angle, radians
q	free-steam dynamic pressure, lb/sq ft
R	Reynolds number based on mean aerodynamic chord of wing
S	total wing area, including portion submerged in body, sq ft
V	free-steam velocity, ft/sec

Subscripts and configuration identification:

T	with transition strip
BW	body and wing
BV	body and vertical tail
BVH	body, vertical tail, and horizontal tail

BWV body, wing, and vertical tail

BWVH body, wing, vertical tail, and horizontal tail

APPARATUS

Wind Tunnel

All tests were conducted in the Langley 9-inch supersonic tunnel, which is a closed-circuit, continuous-operation type in which the stream pressure, temperature, and humidity can be controlled at all times during tunnel operation. Different test Mach numbers are provided by interchangeable nozzle blocks which form test sections approximately 9 inches square. Eleven fine-mesh turbulence-damping screens are installed in the settling chamber ahead of the supersonic nozzle. The turbulence level of the tunnel is considered low, based on past turbulence-level measurements.

Models, Support, and Rolling-Moment Balance

A drawing of the complete 1/63-scale model of the Douglas D-558-II airplane is presented in figure 1. The model was constructed in such a way that the wing could be easily removed, leaving the body-tail configuration. A separate body, identical to the first within machining accuracy, was constructed for the body-wing configuration. The sting was an integral part of the body. The model bodies and the wing were made of steel, and the tail panels were molded from plastic materials. This arrangement of model parts and selection of materials resulted primarily from the necessity for accurately mass-balancing the models.

Some configurations were tested with the canopy in place and some with the canopy removed. When the canopy was removed, the body became a body of revolution.

On both bodies, provision was made for mounting the wing at an angle of incidence of 0°, as well as at an angle of incidence of 3° (the wing-incidence angle for the full-scale airplane). The exact location of the wing for each angle of incidence is given in figure 1.

Since the tail panels were molded from plastic materials, they may have experienced slight bending or twisting when tested. However, the resulting aeroelastic effect on the contributions of the tail panels to C_{l_p} is believed to have been small.

The models were tested in the clean condition and with finely pulverized salt transition strips on the components. The dimensions and locations of the transition strips are given in figure 1.

Photographs of the damping-in-roll test apparatus are presented in figure 2. The model sting was inserted into the spindle of the rolling-moment balance and secured by a Woodruff key and setscrews. The spindle was rotated by means of gears and an electric motor outside the tunnel. The rolling velocity was measured with a Stroboconn frequency indicator which was modified to indicate revolutions per minute by means of a generator attached to the rear of the spindle. The rolling moments were measured by strain gages on the spindle and were transmitted through slip rings and brushes to a Brown self-balancing potentiometer outside the tunnel.

PRECISION

The precision of the data has been determined by estimating the accuracies of the measured quantities and evaluating their effects on the coefficient C_l and the parameter $pb/2V$. Over the range of rolling moments encountered in the tests, the probable error in the strain-gage indication produced an error in C_l of ± 0.00025 for the BWVH, BWV, and BW configurations, and an error of ± 0.00015 for the BVH and BV configurations. Error in the measurement of the rolling velocity caused a maximum error in $pb/2V$ of ± 0.00007. The surveyed variation of each of the free-stream Mach numbers is about ± 0.01, which produced a maximum error in $pb/2V$ of ± 0.00003. Thus, the maximum total error in $pb/2V$ was ± 0.0001. The Reynolds number was accurate to within approximately $\pm 0.01 \times 10^6$.

Model alinement was maintained to within $\pm 0.1^\circ$ of zero pitch and yaw with respect to the tunnel center line. The angle of incidence of the wing was also accurate to within $\pm 0.1^\circ$.

The rolling-moment balance was calibrated statically before and at intervals during the testing to ascertain that there were no changes in the strain-gage constant.

Throughout the tests, the moisture content in the tunnel was kept sufficiently low to insure that the effects of condensation were negligible.

RESULTS AND DISCUSSION

The variations of rolling-moment coefficient with wing-tip helix angle for the various configurations are presented in figures 3 to 10.

It is seen that for the clean configurations, data were obtained only at $M = 1.62$, 1.94, and 2.41 (see figs. 3 to 5), whereas for the configurations with transition strips on the components, data were obtained at $M = 1.62$, 1.94, 2.22, 2.41, and 2.62 (see figs. 6 to 10). At the inception of the test program, investigations were planned only at $M = 1.62$, 1.94, and 2.41. Later the Mach number range of the tests of the models with transition strips on the components was extended to include $M = 2.22$ and 2.62, as a result of the surprising variation of C_{l_p} with M which was obtained for the Bell X-1A research airplane in the Mach number region from 2.22 to 2.41. (See ref. 1.)

Within the accuracy of the data, the variations were quite linear for most of the configurations. However, for several configurations, the variations of C_l with $pb/2V$ were not linear over the entire range of $pb/2V$. (For example, see fig. 3(a), BWVH; fig. 4(a), BW; fig. 4(b), BWVH and BW; and fig. 6(a), BWVH.) These nonlinearities probably represent the net contributions to C_l of thickness effects, separation of the flow near the tips, and aeroelastic effects. All slopes were estimated for the linear portions of the curves; that is, for the partially nonlinear variations cited, the slopes were taken for that portion of the curve which corresponded to the lower values of $pb/2V$.

The variations with Mach number of C_{l_p} for the various configurations are presented in figures 11 to 19. The figures were arranged to show the following: (1) the effects of Reynolds number and boundary layer on C_{l_p}, (2) the effects of wing-incidence angle on C_{l_p}, (3) the contributions of the airplane components to C_{l_p}, and (4) comparisons of the experimental values of C_{l_p} with some theoretical predictions.

The Effects of Reynolds Number and Boundary Layer on C_{l_p}

The variations with Mach number of C_{l_p} for BWVH, BW, and BVH at different Reynolds numbers and with different boundary-layer conditions are presented in figures 11 to 13. The values of C_{l_p} for the clean BWVH and BW configurations were obtained over two Reynolds number ranges for $i_w = 0^\circ$, but over the lower Reynolds number range only for $i_w = 3^\circ$.

The limitation in the testing of the models with $i_w = 3^\circ$ was imposed by the excessive vibration of the model which was encountered over the higher Reynolds number range at relatively low values of rolling velocity. This vibration was caused by the combination of a deflection of the model sting by the lift of the wing and the rolling of the model.

In figures 11, 12, and 13, and in any subsequent figures in which they are presented, the variations of C_{l_p} with M obtained for the clean BWVH, BW, and BVH configurations are dashed in the Mach number region from 1.94 to 2.41 to denote uncertain fairing. This uncertainty resulted from the fact that the clean models were not tested at $M = 2.22$ and 2.62, and the values of C_{l_p} obtained at $M = 2.22$ and 2.62 for the models with transition strips on the components were very influential in determining the variations of C_{l_p} with M for these models.

For BWVH (see fig. 11(a)) and BW (see fig. 12(a)), with $i_w = 0^\circ$, substantial increases in the damping in roll were obtained with increases in Reynolds number. In general, the Reynolds number effect seemed to lessen with increasing Mach number.

For BVH (see fig. 13), the observed changes in C_{l_p} with Reynolds number are believed to lie within the accuracy of determining C_{l_p}. Hence, Reynolds number had practically no effect on C_{l_p} for BVH.

These pronounced Reynolds number effects on C_{l_p} for BWVH and BW suggested the addition of transition strips to the airplane components. The purpose of the transition strips was to create a turbulent boundary layer over most of the model and thereby to simulate more closely full-scale conditions. The effectiveness of similar transition strips in creating a turbulent boundary layer may be seen in reference 2.

Figures 11 and 12 show that for BWVH and BW, with $i_w = 0^\circ$ and 3°, the addition of transition strips to all the components except the body caused increases in the damping at the Mach numbers at which C_{l_p} was obtained with and without transition strips on the components, that is, $M = 1.62$, 1.94, and 2.41. Also apparent in figure 11(b) is the rather large effect of the body transition strip on C_{l_p} for BWVH with $i_w = 3^\circ$.

For BVH, the addition of transition strips to the body and tail panels had little effect on C_{l_p}. (See fig. 13.)

For the tests at the higher Reynolds numbers and for the tests with transition fixed, the resultant increases in extent of turbulent boundary layer had the expected result in increasing the damping of the BWVH and BW configurations. The large effect of the body transition strip on C_{l_p} for BWVH indicates that C_{l_p} for BWVH is very sensitive to changes in the boundary layer over the body. This effect probably can be attributed either to the direct influence of the body boundary layer on the inboard regions of the wing, or to the indirect influence of the body boundary layer on the tail panels by altering the wing loading at the body-wing juncture and thus changing the flow field behind the wing. The effect probably was not due to the direct influence of the body boundary layer on the tail panels, since Reynolds number and boundary layer were shown to have practically no effect on C_{l_p} for BVH.

The Effects of Wing-Incidence Angle on C_{l_p}

The variations with Mach number of C_{l_p} for BWVH and BW at $i_w = 0^\circ$ and $i_w = 3^\circ$ are presented in figures 14 and 15. For the clean models and the transition-strip models of BWVH and BW, changing the wing-incidence angle from 3° to 0° produced decreases in the damping at $M = 1.62$ and $M = 1.94$, but had very little effect at $M = 2.41$. Comparison of the results of figures 14(a) and 14(b) shows that for the clean models the wing was predominant in effecting the changes in C_{l_p} with i_w. The results of figure 15 indicate that for the transition-strip models the decrease in damping with increasing wing-incidence angle was primarily due to the tail panels.

The Contributions of the Airplane Components to C_{l_p}

The variations with Mach number of C_{l_p} for the complete model and combinations of its components are presented in figures 16 and 17. Also presented are some variations of C_{l_p} with Mach number obtained by adding values of C_{l_p} for certain combinations of components. Comparisons of the variations for the complete configurations with variations obtained by adding the values of C_{l_p} for the body-wing and body—vertical-tail—horizontal-tail combinations in figures 16 and 17(a) show that, for the clean models with $i_w = 0^\circ$ and 3° and for the transition-strip models

with $i_w = 0^\circ$, the contributions of the tail panels to C_{l_p} were partially nullified by the flow field behind the wing and by other interference effects.

Figures 17(b) and 17(c) show that with $i_w = 3^\circ$ and transition strips on all components except the body, all configurations containing the wing experienced rather abrupt losses in damping in roll near $M = 2.22$. The variation of C_{l_p} with M for $BW_TV_TH_T$ corresponded quite closely to that obtained by adding C_{l_p} for BW_T and $B_TV_TH_T$, and the variation of C_{l_p} with M for BW_TV_T was in fair agreement with that obtained by adding C_{l_p} for BW_T and B_TV_T. This type of addition and comparison is justified by the fact that Reynolds number and boundary layer had little effect on the damping of the BVH combination. (See fig. 13.) Thus there were no large effects of wing-tail interference on C_{l_p} for $BW_TV_TH_T$ and BW_TV_T. The somewhat different variation of C_{l_p} with M obtained for $B_TW_TV_TH_T$ is probably more nearly applicable to the full-scale airplane, since the boundary layer along the body ahead of the body-wing juncture was turbulent for $B_TW_TV_TH_T$, whereas it was probably laminar for $BW_TV_TH_T$. The configurations $B_TW_TV_TH_T$ and BW_TV_T were also tested with the canopy in place, and the results showed little effect of the canopy on C_{l_p} for either configuration.

Comparisons of the Experimental Values of C_{l_p} With Some Theoretical Predictions

The experimental variations of C_{l_p} with M are compared with some theoretical variations for the complete model and its components in figures 18 and 19. All theoretical predictions, except the limited variations for BWVH taken from references 3 and 4 (see fig. 18(b)), were obtained by the method of reference 2. This method consisted of predictions by the linear theory of references 5 and 6 of C_{l_p} for the wing and tail panels (giving the variations for BW, BV, and BVH presented in fig. 19) plus approximations of the effects of the wing flow field on the damping of the tail panels. The effect of the interference field from the body was neglected, and the wing was assumed to have zero dihedral and zero incidence. No theoretical predictions by the method of reference 2 of C_{l_p} for BWVH and BWV are shown in figure 18 for $M < 1.94$ because the technique for approximating the effects of the wing flow field on the

damping of the tail panels was not applicable to the Douglas D-558-II airplane at Mach numbers lower than about 1.94.

In figure 18(a), it is seen that with $i_w = 0^\circ$, the damping in roll of the $BW_TV_TH_T$ configuration agreed fairly well with the theoretical predictions at $M = 1.94$ and $M = 2.41$, whereas the damping of the clean BWVH models was considerably lower than that predicted by theory.

Figure 18(b) shows that with $i_w = 3^\circ$ the general levels and trends of the experimental variations of C_{l_p} with M for the complete configuration and the body—wing—vertical-tail configuration were adequately predicted by the available theories.

Figure 19(a) shows that with $i_w = 0^\circ$, good agreement between theory and experiment was obtained for the body-wing configuration at $M = 2.41$, but that theory overestimated the damping by progressively larger amounts as the Mach number decreased to 1.94 and 1.62, both for the clean model and for the transition-strip model. Also, theory overestimated the damping by progressively larger amounts when the transition strips were removed and as the Reynolds number decreased for the clean model. The good agreement between theory and experiment at $M = 2.41$ and the progressively increasing overestimation by theory at the lower Mach numbers is consistent with the results obtained for swept, tapered wings in reference 7. In reference 7, the experimental damping in roll was considerably lower than the theoretical damping when the wing leading edges were in the vicinity of or behind the Mach cone from the wing apex, and the discrepancy became less when the leading edges were ahead of the Mach cone. In the present investigation, the leading edges of the wing were in the vicinity of the Mach cone at $M = 1.62$, and were ahead of the Mach cone at $M = 1.94$ and $M = 2.41$.

In figure 19(b) it is seen that the damping of the body-wing, body—vertical-tail—horizontal-tail, and body—vertical-tail configurations was adequately predicted by theory, with the exception of the body-wing configuration at $M = 1.62$ and $M = 2.22$, for which theory overestimated the damping.

CONCLUDING REMARKS

Wind-tunnel investigations of the damping in roll at zero angle of attack of the Douglas D-558-II research airplane and its components were made at Mach numbers of 1.62, 1.94, 2.22, 2.41, and 2.62.

The general levels and trends of the variations of the damping in roll C_{l_p} with Mach number for the complete model and its components

were of the order predicted by theory. For some configurations, the contributions of the tail panels to C_{l_p} were partially nullified by the flow field behind the wing and other interference effects. The canopy was found to have little effect on the damping in roll.

Increasing the Reynolds number produced substantial increases in the damping in roll of the complete model and the body-wing model. In most cases, the addition of transition strips to the components resulted in further increases in the damping. For the complete model, C_{l_p} was very sensitive to changes in the boundary layer over the body. Changing the wing incidence angle from 3° to 0° decreased the damping at the lower Mach numbers.

Langley Aeronautical Laboratory,
National Advisory Committee for Aeronautics,
Langley Field, Va., May 16, 1956.

REFERENCES

1. McDearmon, Russell W., and Clark, Frank L.: Wind-Tunnel Investigation of the Damping in Roll of the Bell X-1A Research Ariplane and Its Components at Supersonic Speeds. NACA RM L55I19, 1956.

2. Fallis, William B.: On Distributed Roughness as a Means of Fixing Transition at High Supersonic Speeds. Jour. Aero. Sci. (Readers' Forum), vol. 22, no. 5, May 1955, p. 339.

3. Queijo, M. J., and Goodman, Alex: Calculations of the Dynamic Lateral Stability Characteristics of the Douglas D-558-II Airplane in High-Speed Flight for Various Wing Loadings and Altitudes. NACA RM L50H16a, 1950.

4. Ankenbruck, Herman O., and Wolowicz, Chester H.: Lateral Motions Encountered With the Douglas D-558-II All-Rocket Research Airplane During Exploratory Flights to a Mach Number of 2.0. NACA RM H54I27, 1954.

5. Harmon, Sidney M., and Jeffreys, Isabella: Theoretical Lift and Damping in Roll of Thin Wings With Arbitrary Sweep and Taper at Supersonic Speeds - Supersonic Leading and Trailing Edges. NACA TN 2114, 1950.

6. Malvestuto, Frank S., Jr., Margolis, Kenneth, and Ribner, Herbert S.: Theoretical Lift and Damping in Roll at Supersonic Speeds of Thin Sweptback Tapered Wings With Streamwise Tips, Subsonic Leading Edges, and Supersonic Trailing Edges. NACA Rep. 970, 1950. (Supersedes NACA TN 1860.)

7. McDearmon, Russell W., and Heinke, Harry S., Jr.: Investigations of the Damping in Roll of Swept and Tapered Wings at Supersonic Speeds. NACA RM L53A13, 1953.

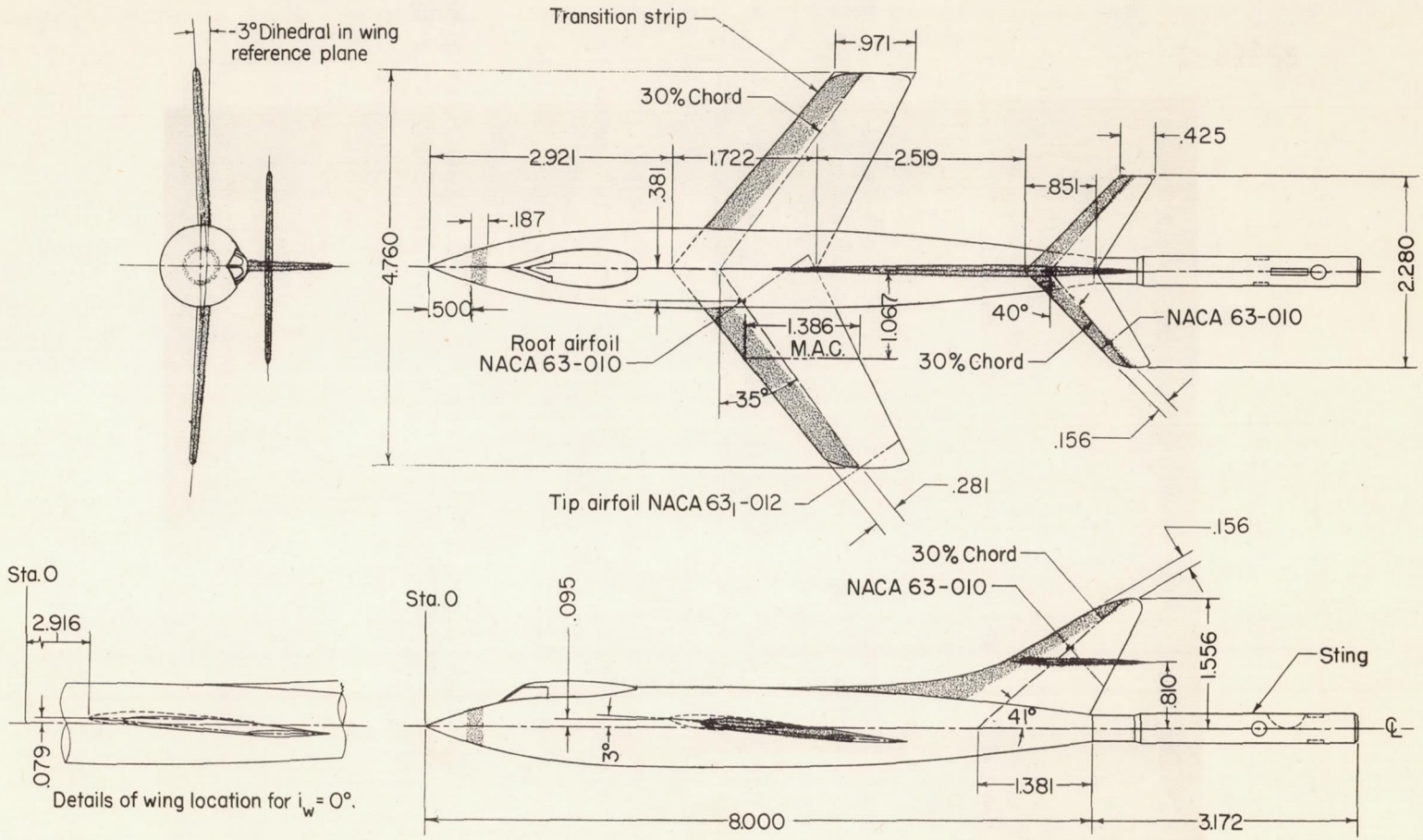

Figure 1.- Drawing of the complete model. All dimensions are in inches.

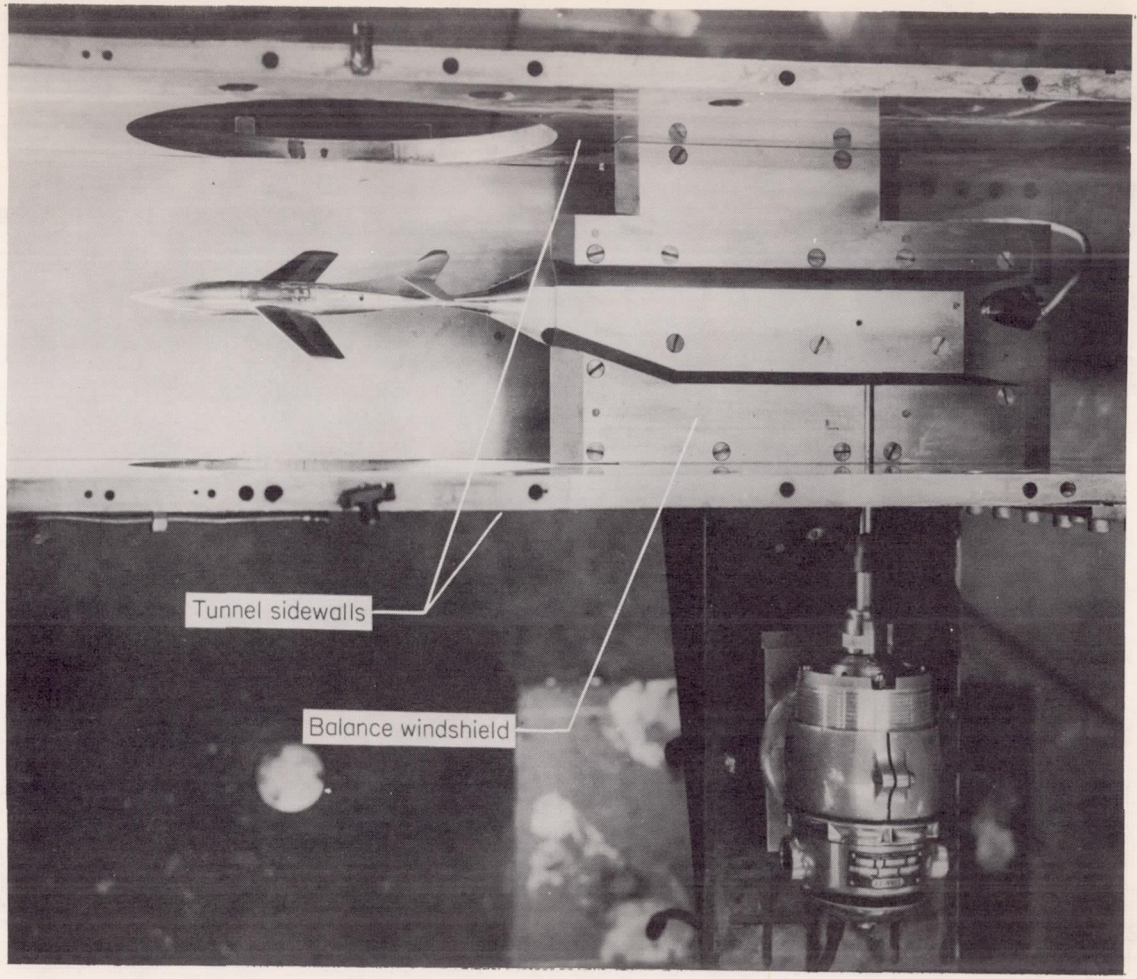

(a) Setup in tunnel (top nozzle block removed). L-93522

Figure 2.- Photographs of the damping-in-roll test apparatus and the complete model.

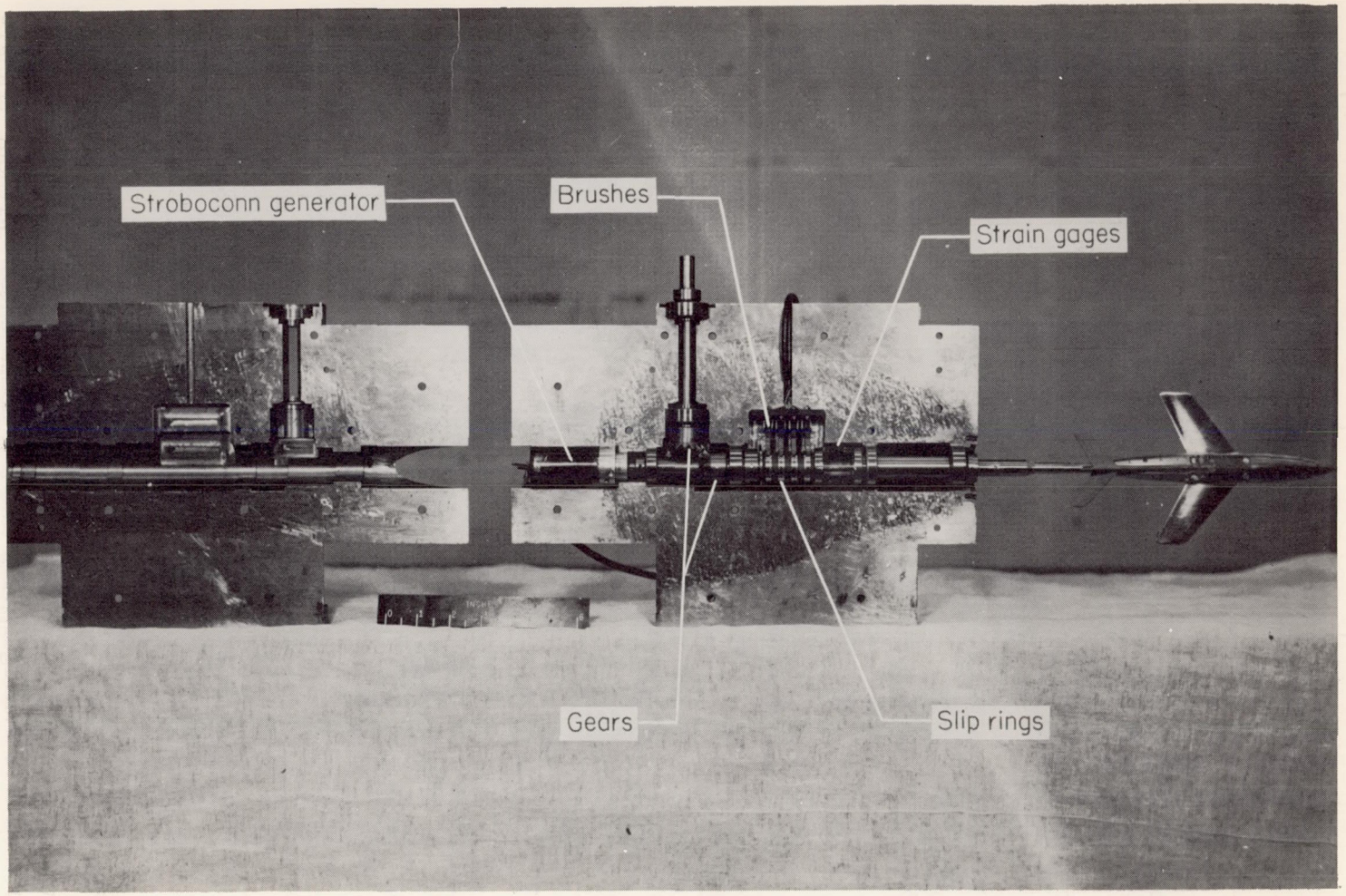

L-93523

(b) Interior of balance.

Figure 2.- Concluded.

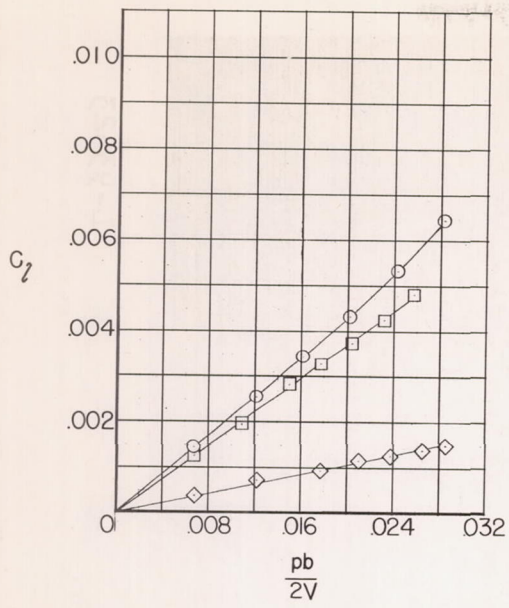

(a) $i_w = 0°$; $R = 0.49 \times 10^6$.

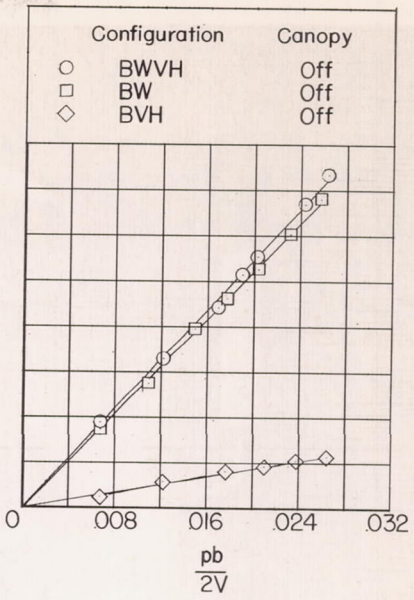

(b) $i_w = 0°$; $R = 0.96 \times 10^6$.

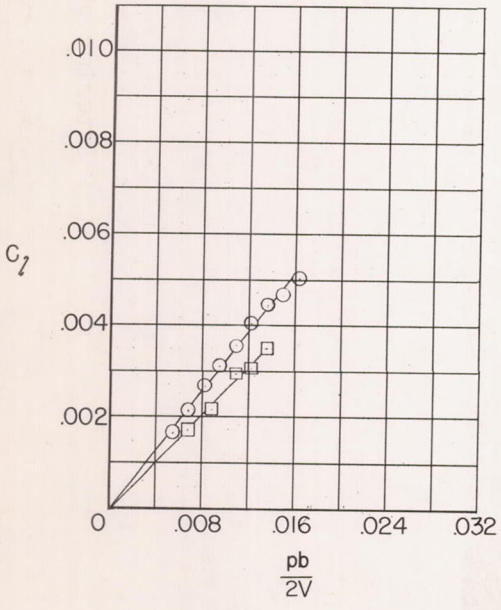

(c) $i_w = 3°$; $R = 0.49 \times 10^6$.

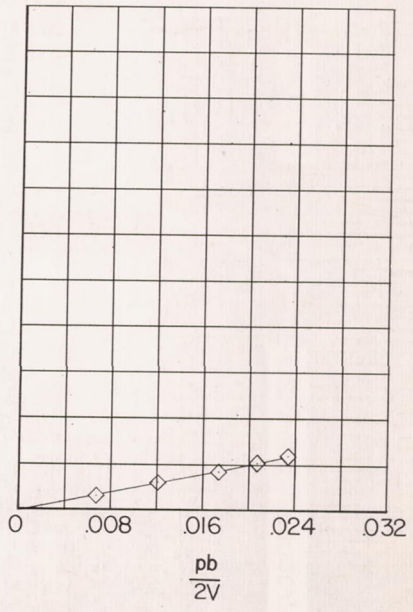

(d) $R = 1.52 \times 10^6$.

Figure 3.- Variations of rolling-moment coefficient with wing-tip helix angle for complete configuration and its components. Without transition strips; M = 1.62.

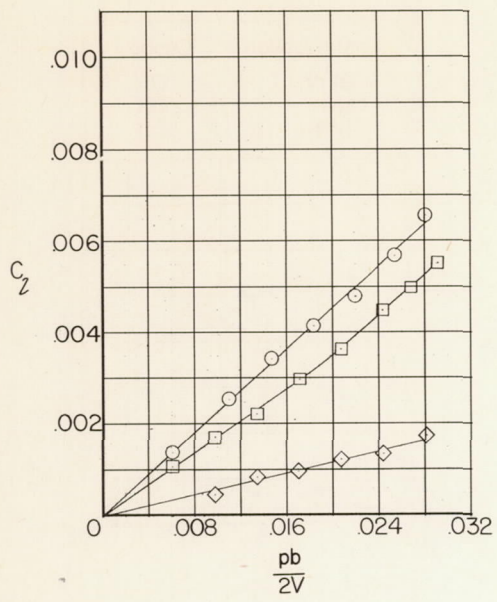

(a) $i_w = 0°$; $R = 0.44 \times 10^6$.

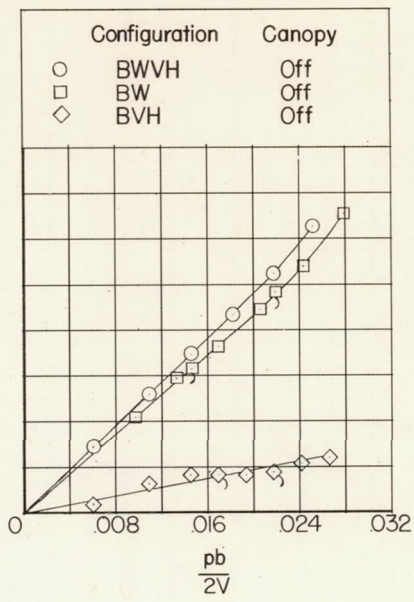

(b) $i_w = 0°$; $R = 0.85 \times 10^6$.

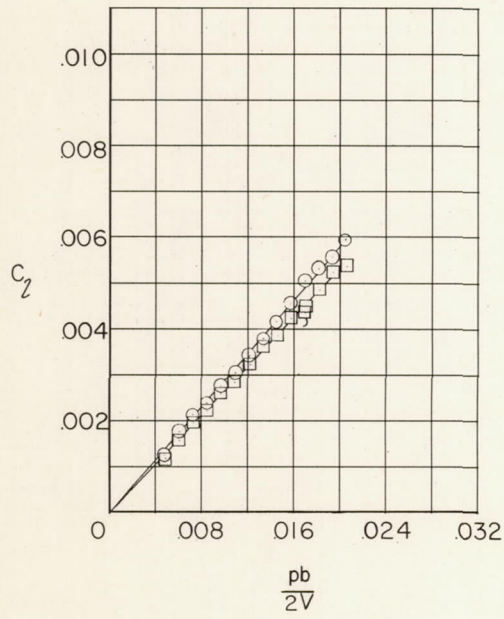

(c) $i_w = 3°$; $R = 0.43 \times 10^6$.

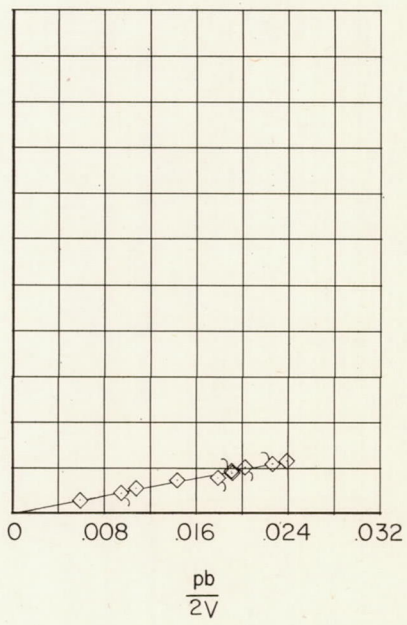

(d) $R = 1.48 \times 10^6$.

Figure 4.- Variations of rolling-moment coefficient with wing-tip helix angle for complete configuration and its components. Without transition strips; M = 1.94. Flagged symbols indicate check points.

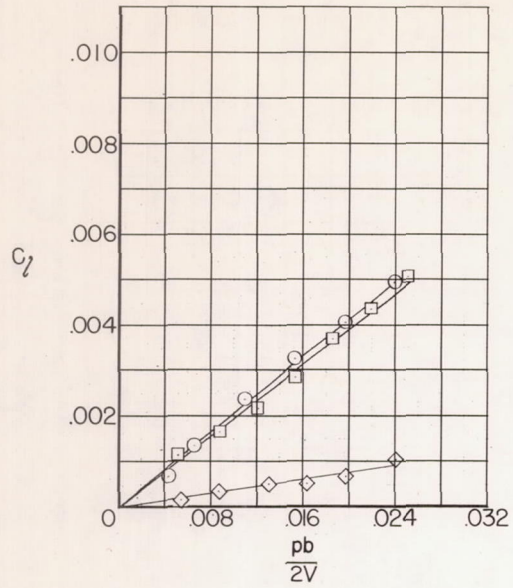

(a) $i_w = 0°$; $R = 0.36 \times 10^6$.

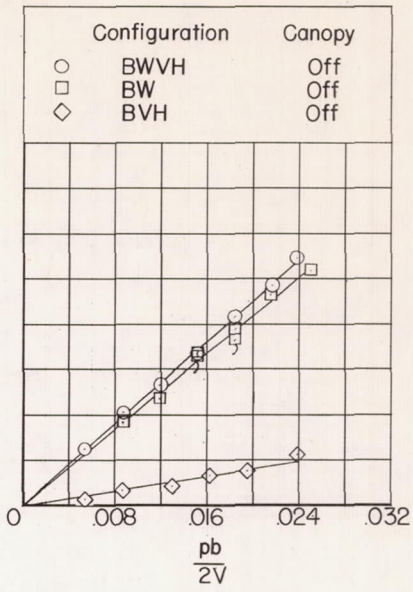

(b) $i_w = 0°$; $R = 0.69 \times 10^6$.

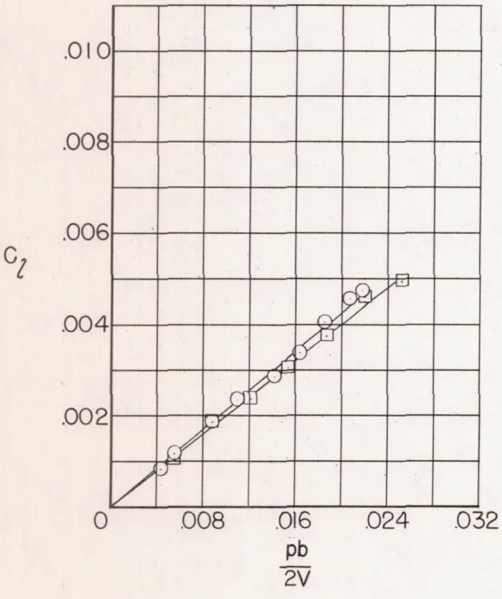

(c) $i_w = 3°$; $R = 0.36 \times 10^6$.

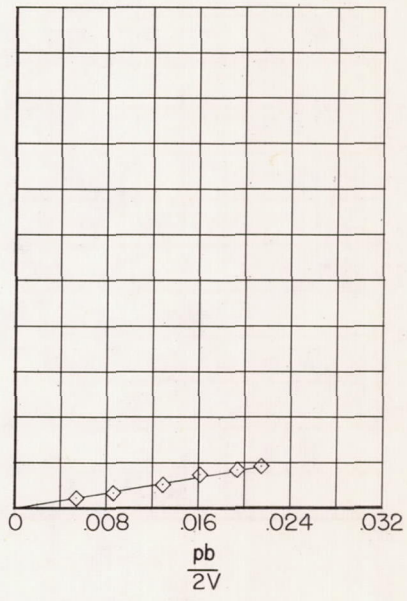

(d) $R = 1.33 \times 10^6$.

Figure 5.- Variations of rolling-moment coefficient with wing-tip helix angle for complete configuration and its components. Without transition strips; M = 2.41. Flagged symbols indicate check points.

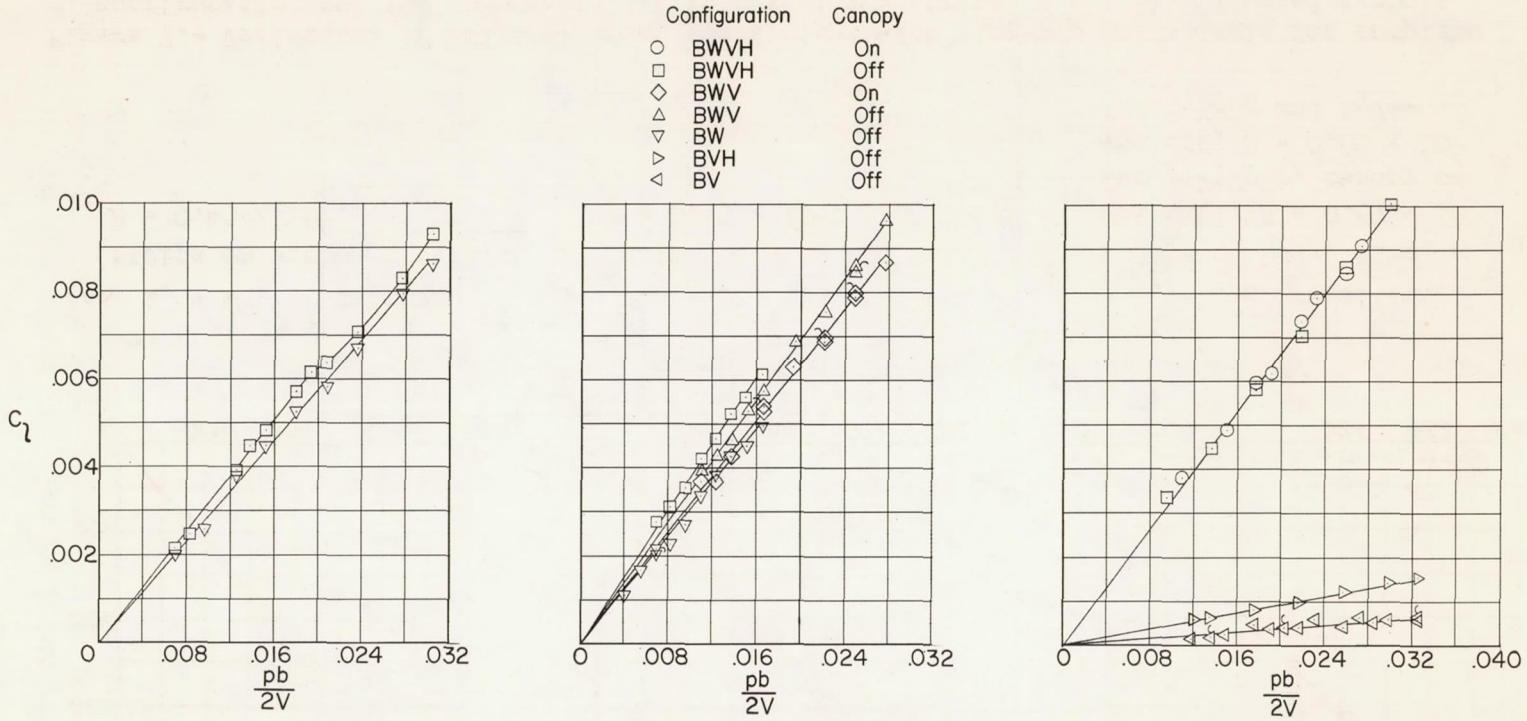

(a) $i_W = 0^\circ$; transition strips on wing and tail; $R = 0.50 \times 10^6$.

(b) $i_W = 3^\circ$; transition strips on wing and tail; $R = 0.50 \times 10^6$.

(c) $i_W = 3^\circ$; transition strips on body, wing, and tail; $R = 0.50 \times 10^6$ for $B_T W_T V_T H_T$, canopy on and off; $R = 0.95 \times 10^6$ for $B_T V_T H_T$ and $B_T V_T$.

Figure 6.- Variations of rolling-moment coefficient with wing-tip helix angle for complete configuration and its components. With transition strips; M = 1.62. Flagged symbols indicate check points.

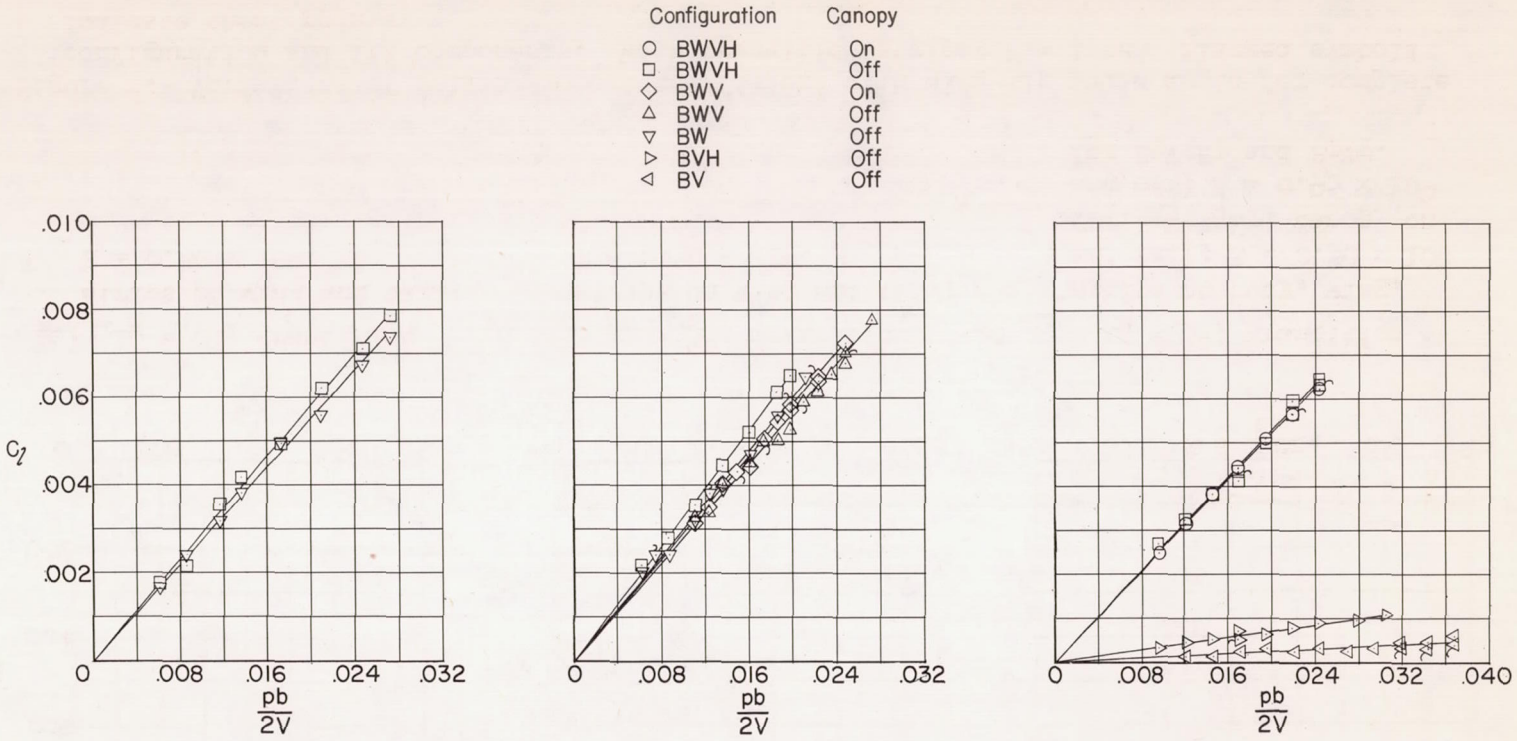

(a) $i_w = 0^\circ$; transition strips on wing and tail; $R = 0.45 \times 10^6$.

(b) $i_w = 3^\circ$; transition strips on wing and tail; $R = 0.45 \times 10^6$.

(c) $i_w = 3^\circ$; transition strips on body, wing, and tail; $R = 0.57 \times 10^6$ for $B_T W_T V_T H_T$, canopy on and off; $R = 0.86 \times 10^6$ for $B_T V_T H_T$ and $B_T V_T$.

Figure 7.- Variations of rolling-moment coefficient with wing-tip helix angle for complete configuration and its components. With transition strips; M = 1.94. Flagged symbols indicate check points.

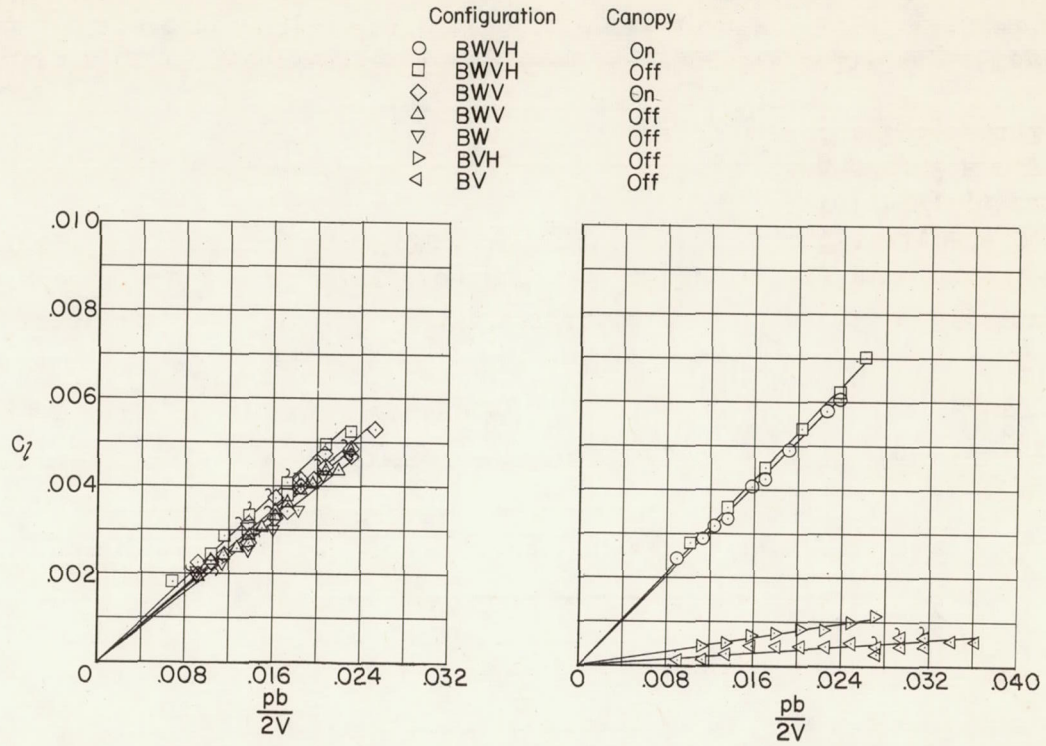

(a) $i_w = 3^\circ$; transition strips on wing and tail; $R = 0.41 \times 10^6$.

(b) $i_w = 3^\circ$; transition strips on body, wing, and tail; $R = 0.64 \times 10^6$ for $B_T W_T V_T H_T$, canopy on and off; $R = 0.76 \times 10^6$ for $B_T V_T H_T$ and $B_T V_T$.

Figure 8.- Variations of rolling-moment coefficient with wing-tip helix angle for complete configuration and its components. With transition strips; M = 2.22. Flagged symbols indicate check points.

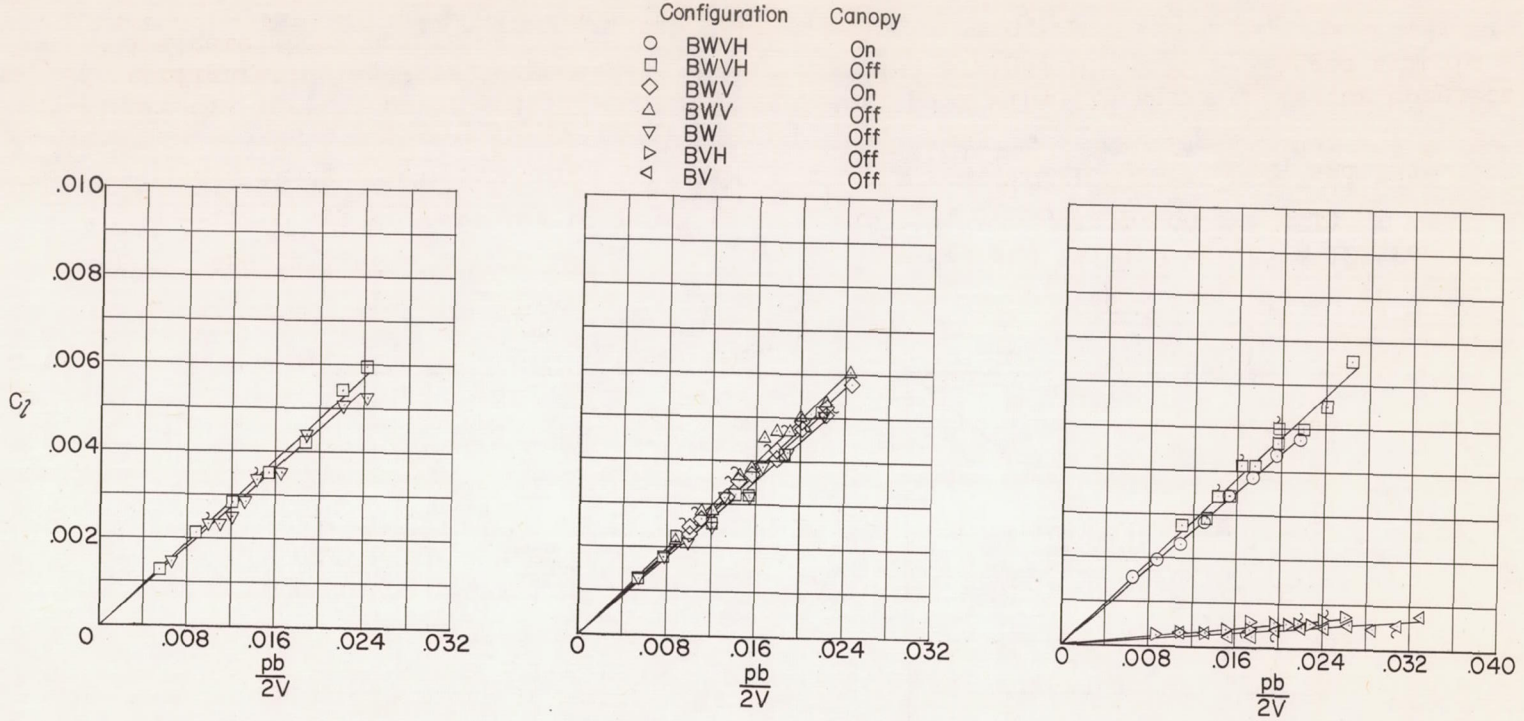

(a) $i_w = 0^\circ$; transition strips on wing and tail; $R = 0.36 \times 10^6$.

(b) $i_w = 3^\circ$; transition strips on wing and tail; $R = 0.36 \times 10^6$.

(c) $i_w = 3^\circ$; transition strips on body, wing, and tail; $R = 0.36 \times 10^6$ for $B_T W_T V_T H_T$, canopy on and off; $R = 0.73 \times 10^6$ for $B_T V_T H_T$ and $B_T V_T$.

Figure 9.- Variations of rolling-moment coefficient with wing-tip helix angle for complete configuration and its components. With transition strips; M = 2.41. Flagged symbols indicate check points.

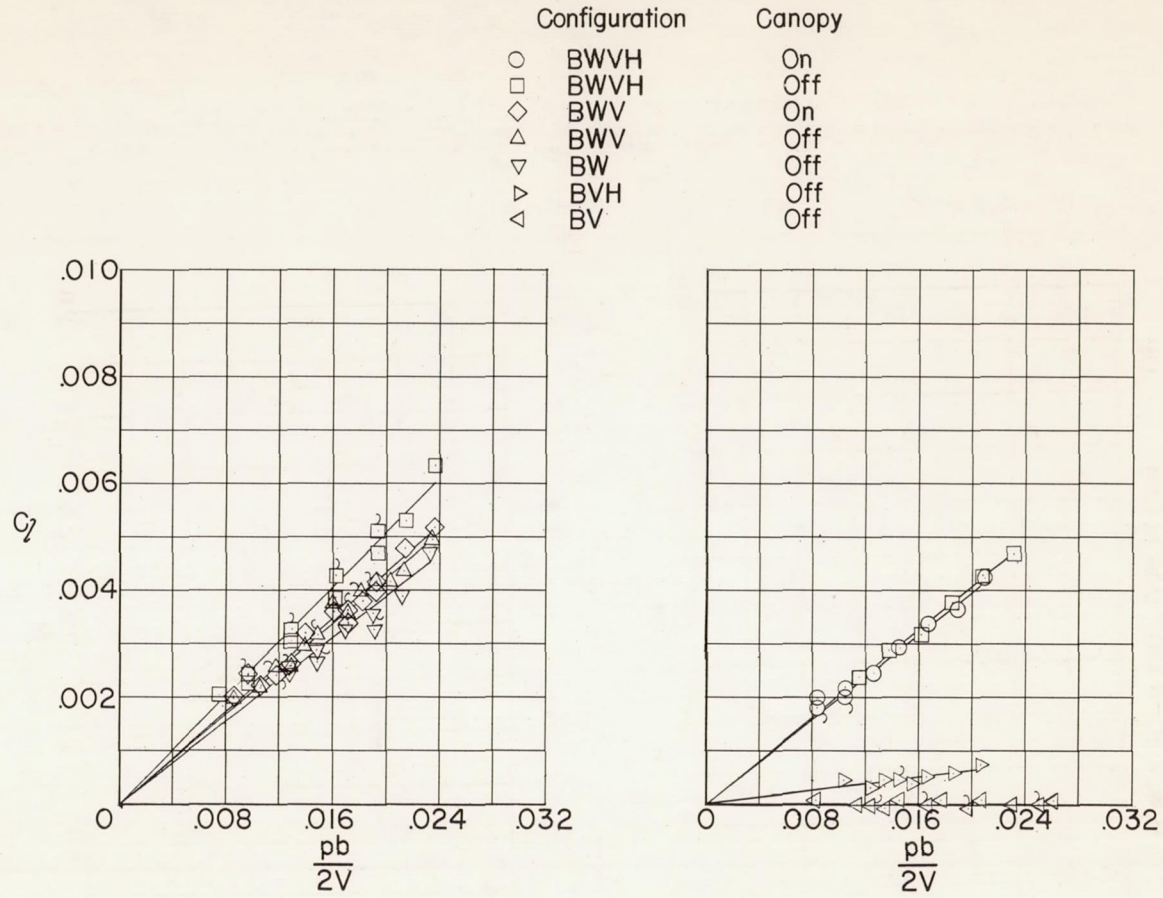

(a) $i_w = 3^\circ$; transition strips on wing and tail; $R = 0.33 \times 10^6$.

(b) $i_w = 3^\circ$; transition strips on body, wing, and tail; $R = 0.64 \times 10^6$ for $B_T W_T V_T H_T$, canopy on and off; $R = 0.90 \times 10^6$ for $B_T V_T H_T$ and $B_T V_T$.

Figure 10.- Variations of rolling-moment coefficient with wing-tip helix angle for complete configuration and its components. With transition strips; M = 2.62. Flagged symbols indicate check points.

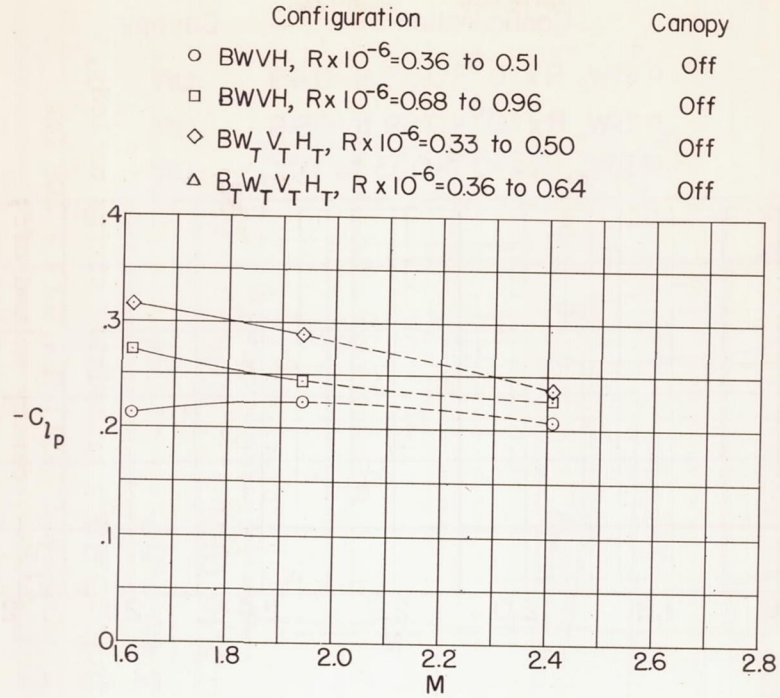

(a) $i_w = 0^\circ$.

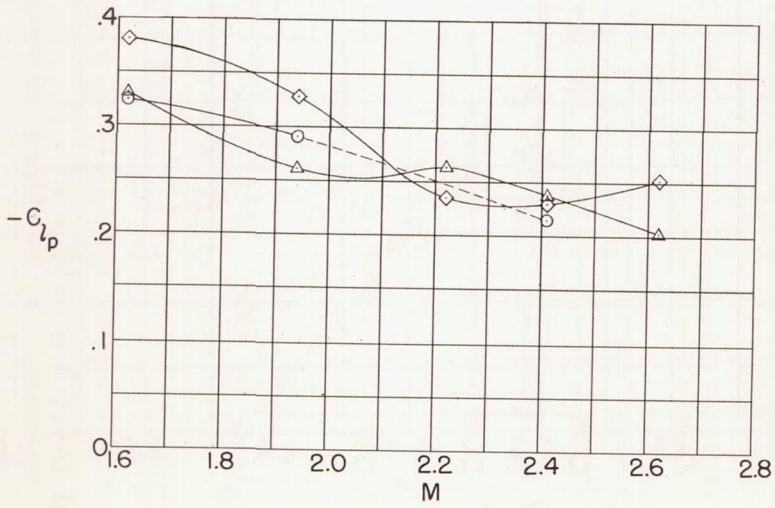

(b) $i_w = 3^\circ$.

Figure 11.- Variations with Mach number of the damping in roll for BWVH at different Reynolds numbers and with different boundary-layer conditions. Dashed portions of curves denote uncertain fairing.

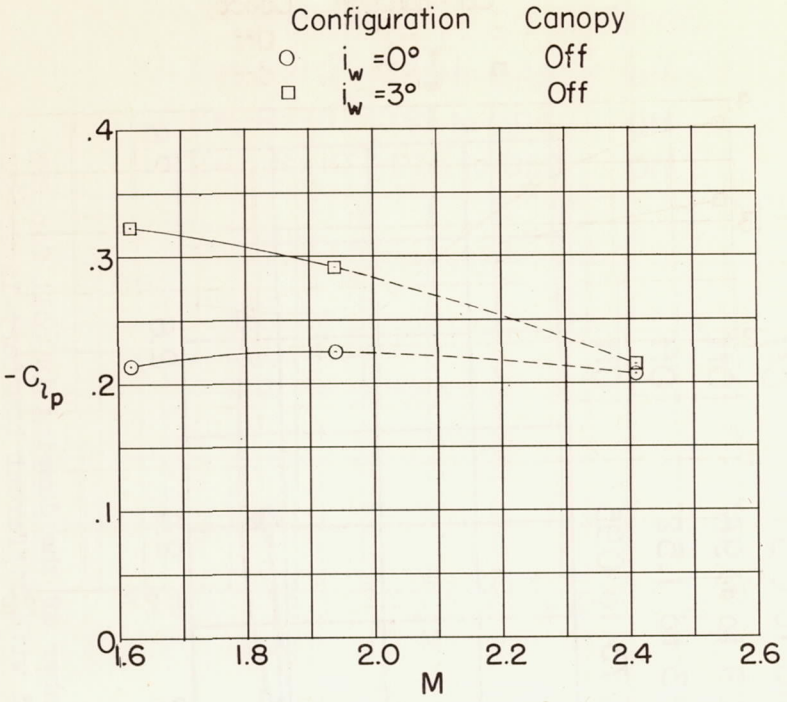

(a) BWVH.

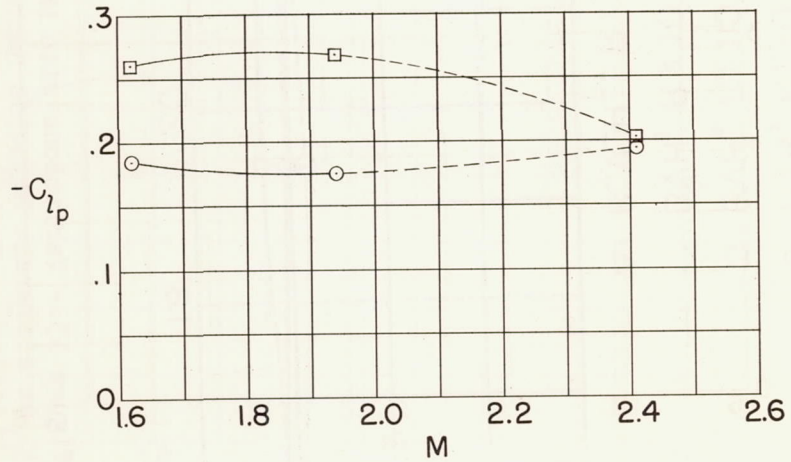

(b) BW.

Figure 14.- Variations with Mach number of the damping in roll for BWVH and BW with different angles of wing incidence. Without transition strips; R = 0.36 to 0.50 × 10^6. Dashed portions of curves denote uncertain fairing.

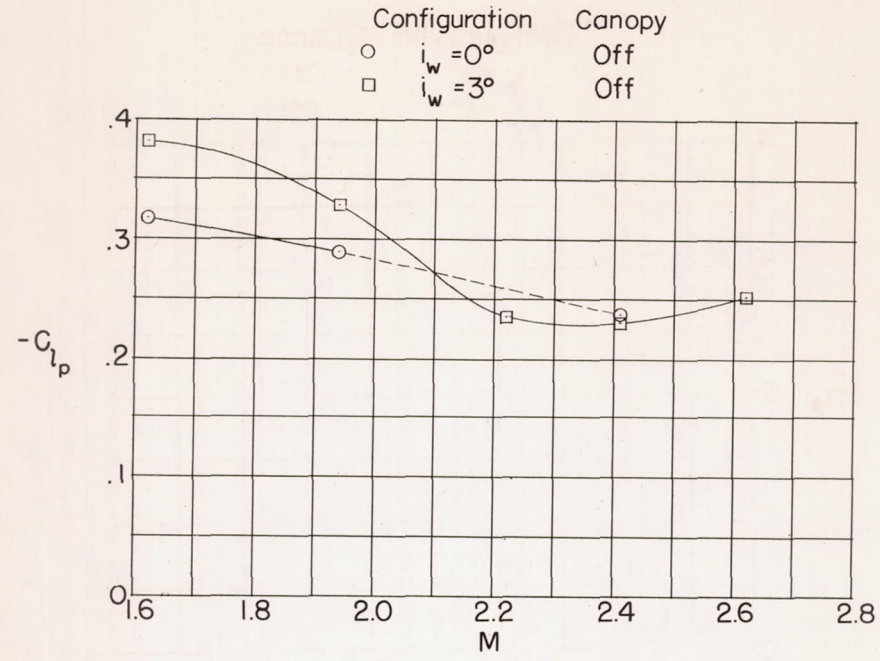

(a) $BW_TV_TH_T$.

(b) BW_T.

Figure 15.- Variations with Mach number of the damping in roll for BWVH and BW with different angles of wing incidence. With transition strips on wing and tail; R = 0.33 to 0.50 × 10^6. Dashed portions of curves denote uncertain fairing.

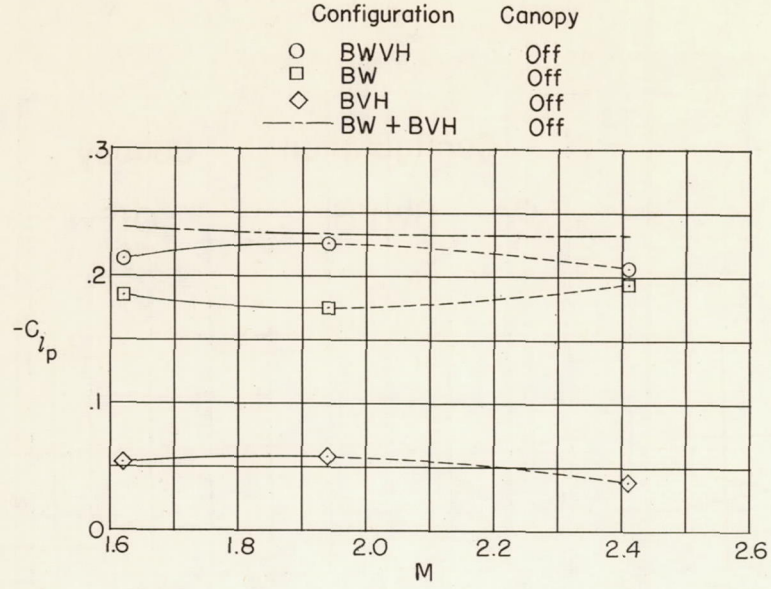

(a) $i_w = 0^\circ$; R = 0.35 to 0.50 $\times 10^6$.

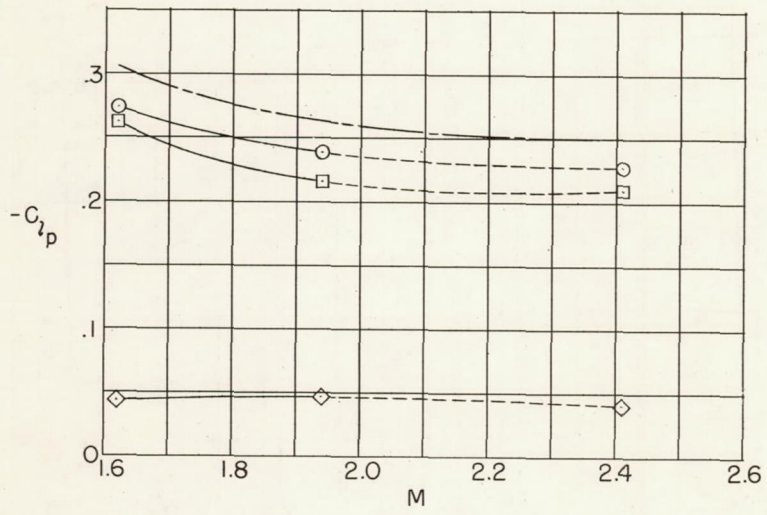

(b) $i_w = 0^\circ$; R = 0.69 to 0.96 $\times 10^6$.

Figure 16.- Variations with Mach number of the damping in roll of the complete model and its components. Without transition strips. Dashed portions of curves denote uncertain fairing.

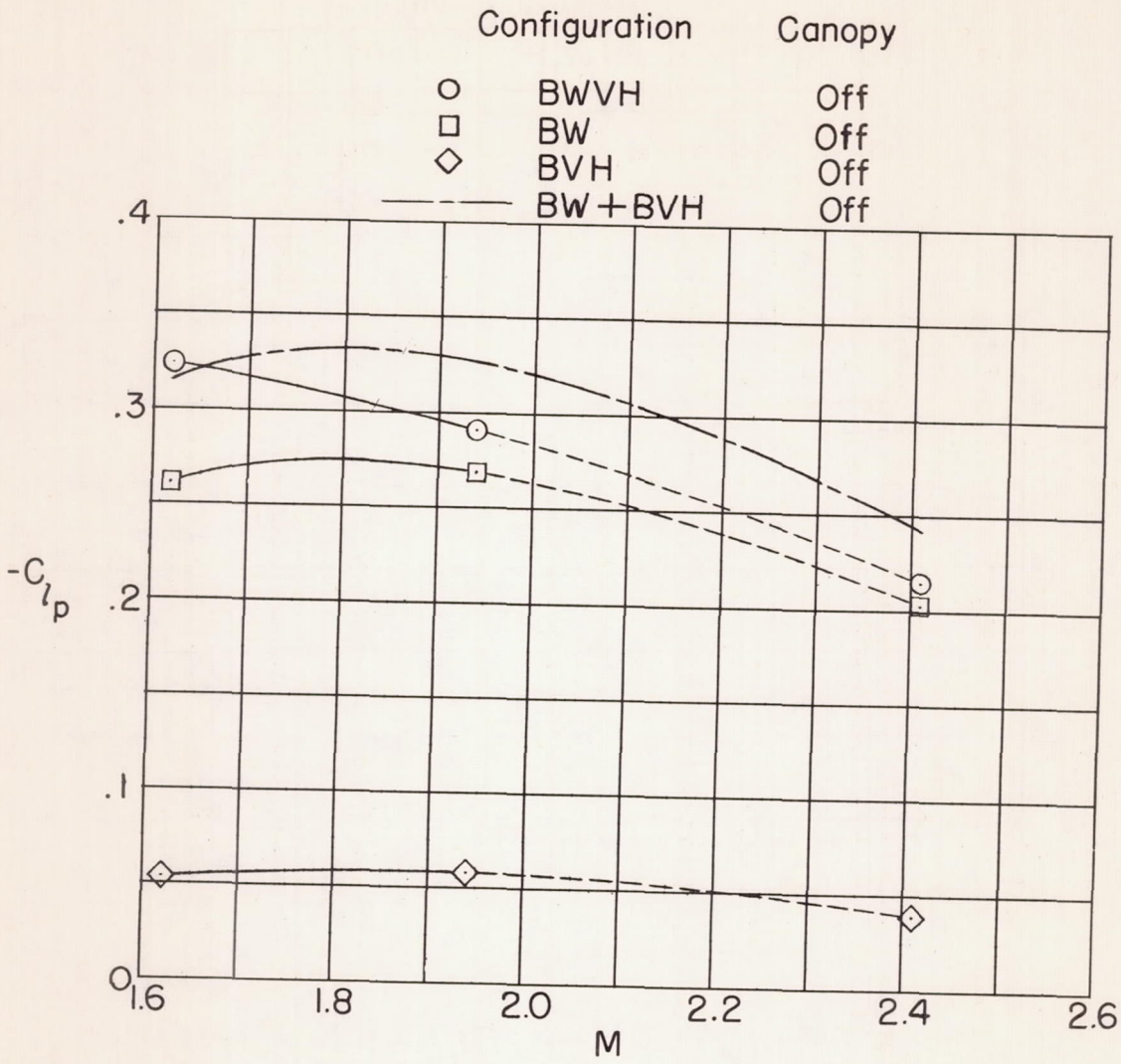

(c) $i_w = 3^o$; R = 0.36 to 0.51 x 10^6.

Figure 16.- Concluded.

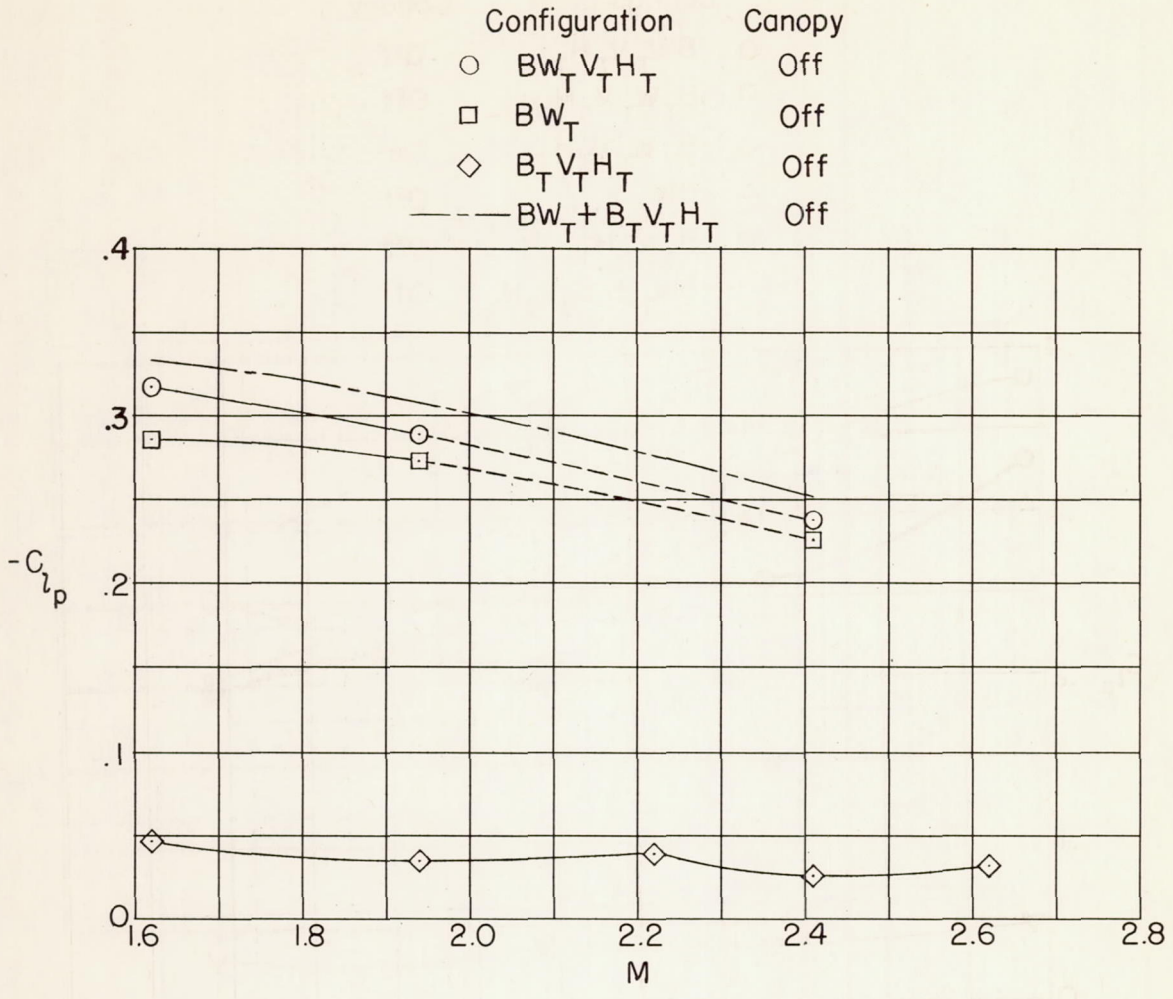

(a) $i_w = 0^\circ$. BWVH, BW, and BVH; R = 0.36 to 0.95 $\times 10^6$.

Figure 17.- Variations with Mach number of the damping in roll of the complete model and its components. With transition strips. Dashed portions of curves denote uncertain fairing.

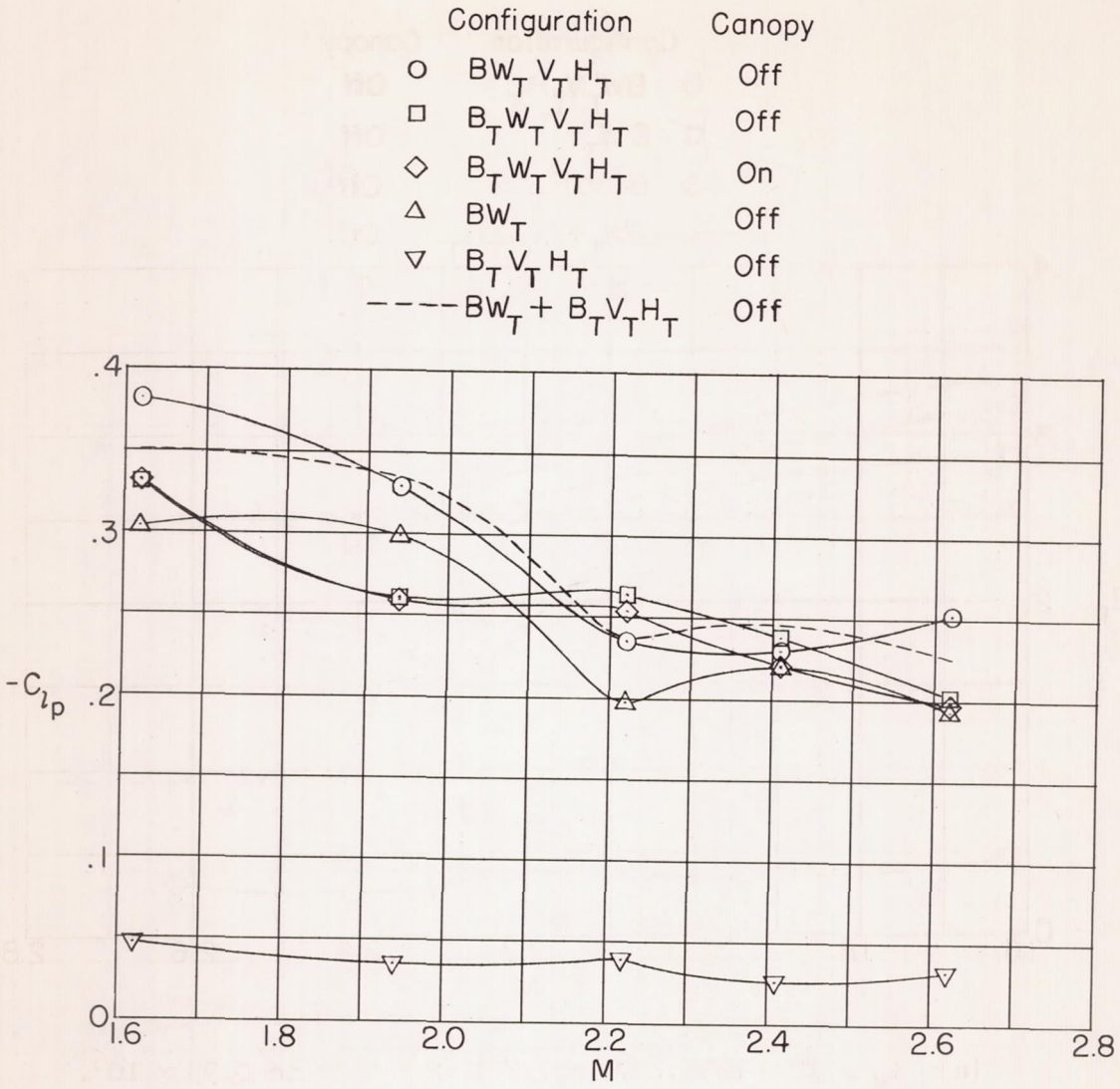

(b) $i_W = 3^\circ$. BWVH, BW, and BVH; R = 0.33 to 0.95 x 10^6.

Figure 17.- Continued.

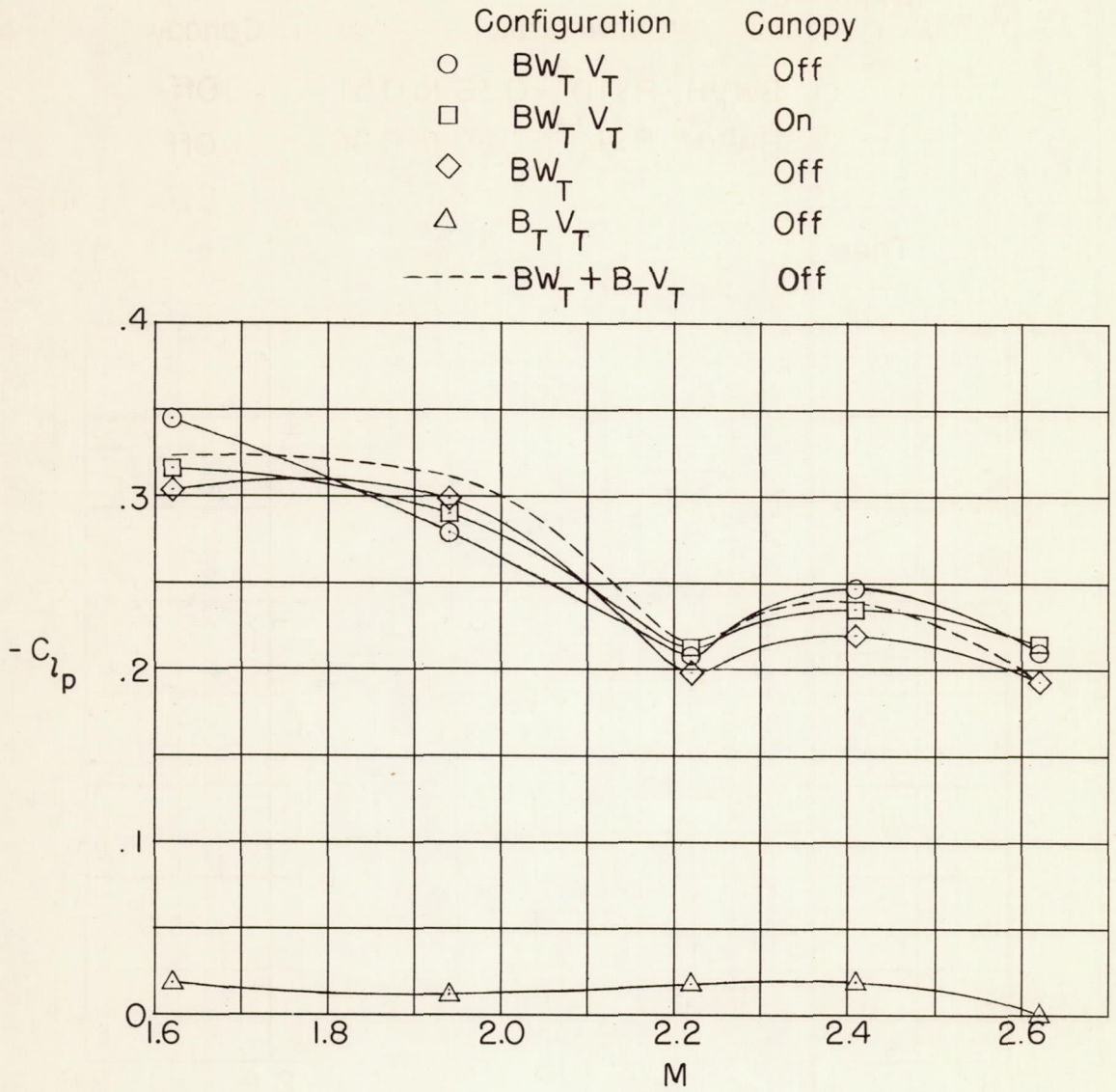

(c) $i_w = 3^\circ$. BWV, BW, and BV; R = 0.33 to 0.95 $\times 10^6$.

Figure 17.- Concluded.

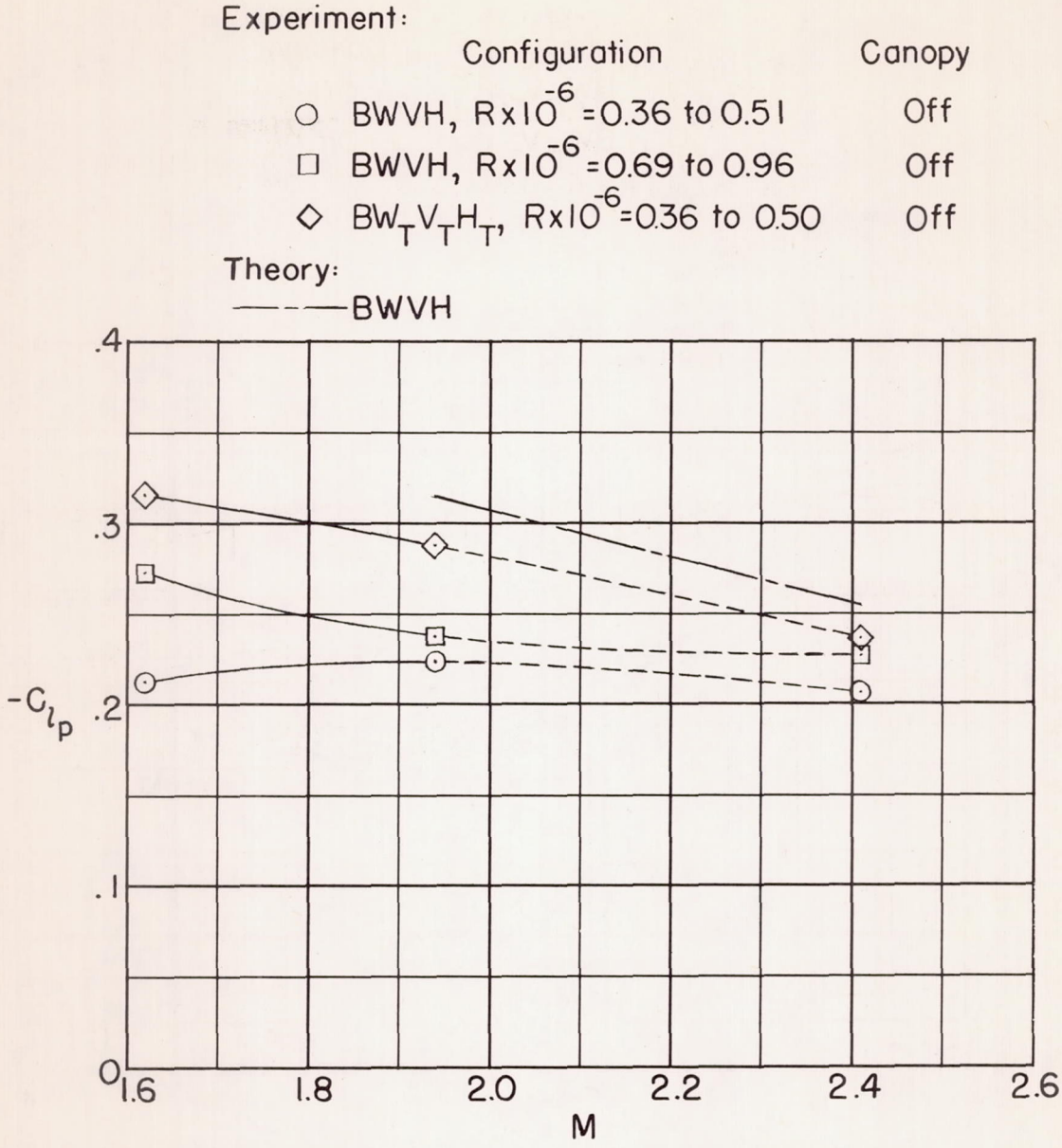

(a) $i_W = 0^\circ$.

Figure 18.- Variations with Mach number of the experimental and theoretical damping in roll for BWVH and BWV. Dashed portions of experimental curves denote uncertain fairing.

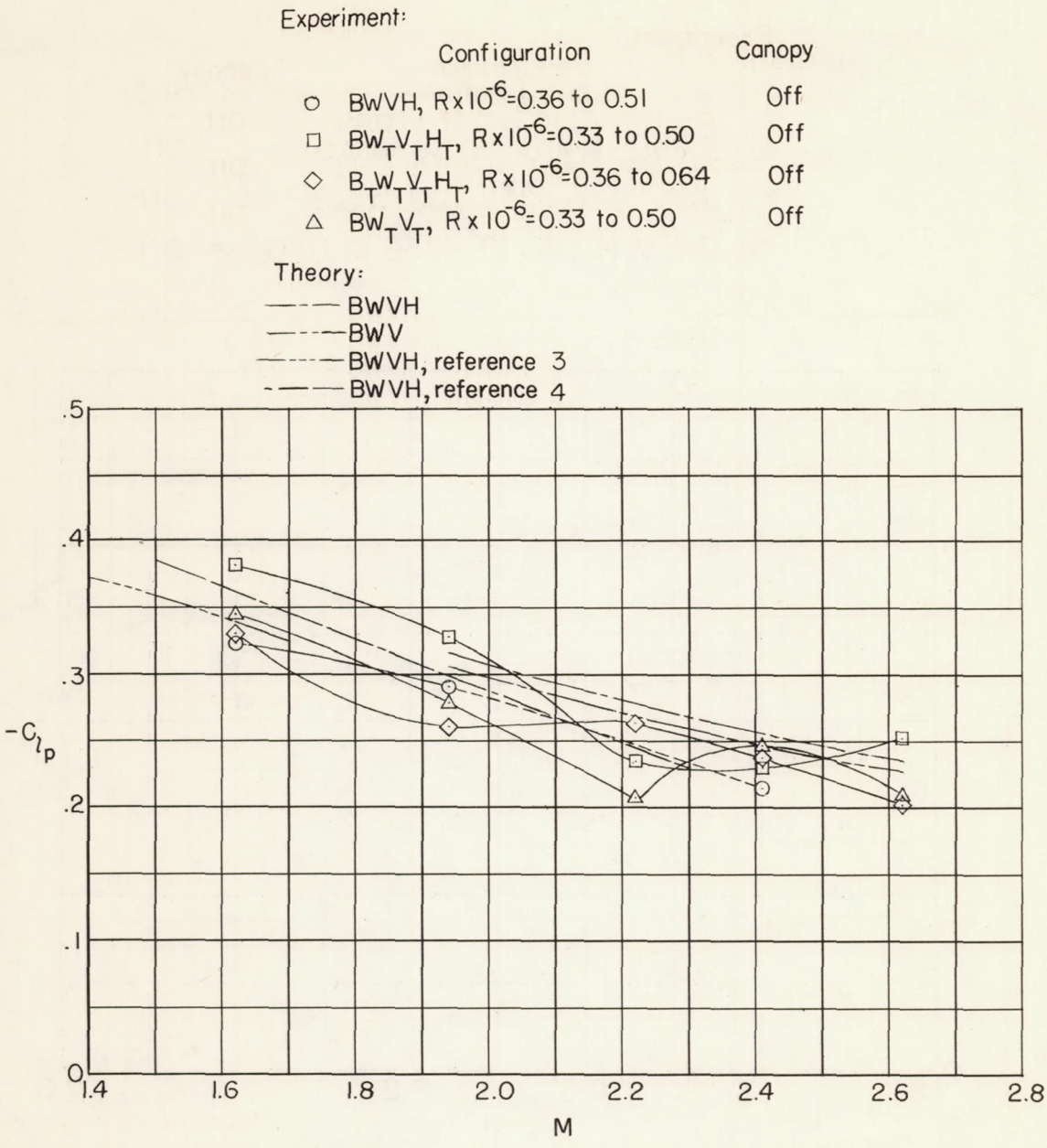

(b) $i_w = 3^\circ$.

Figure 18.- Concluded.

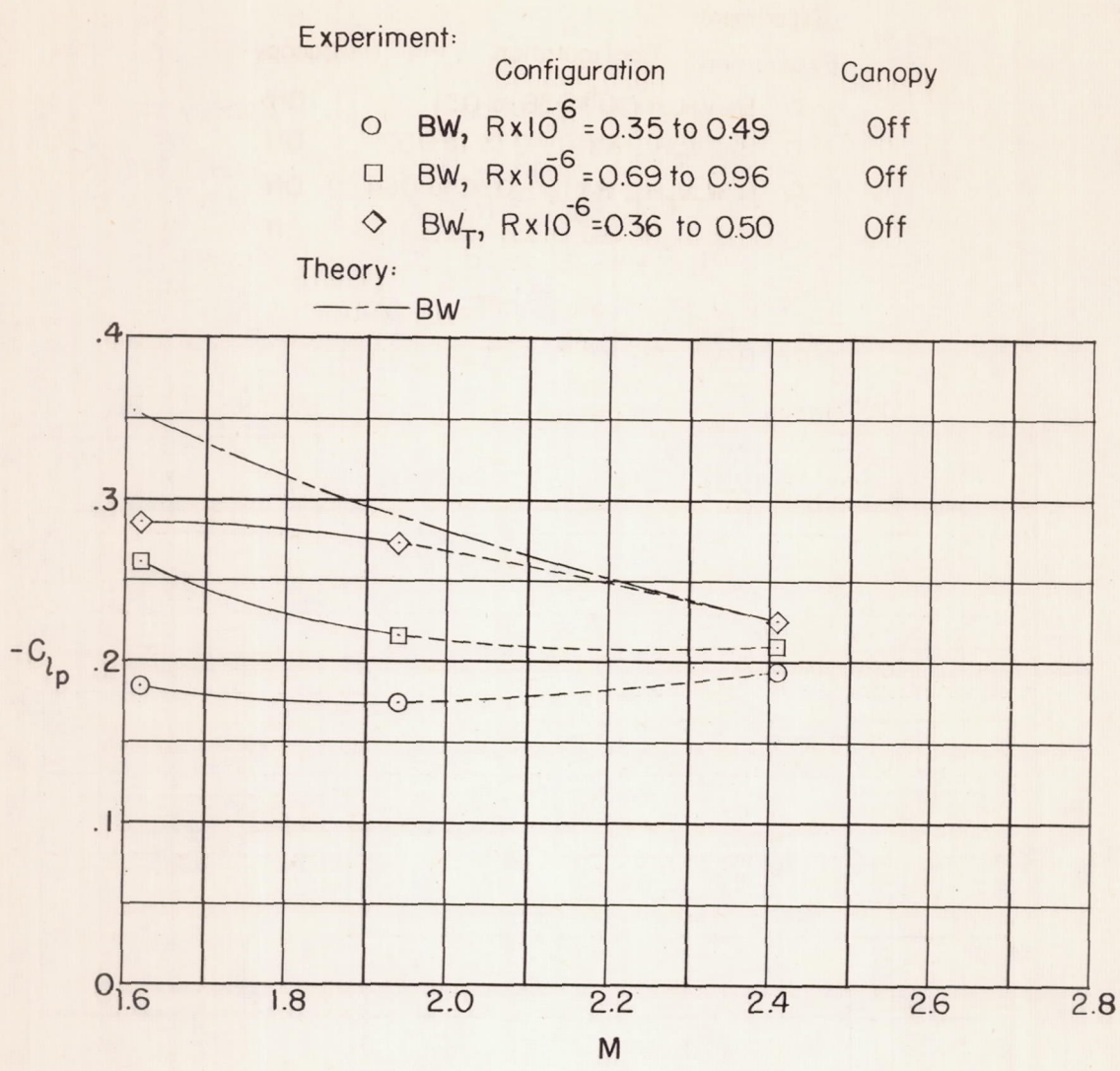

(a) $i_W = 0^\circ$.

Figure 19.- Variations with Mach number of the experimental and theoretical damping in roll for BW, BVH, and BV. Dashed portions of experimental curves denote uncertain fairing.

Experiment:

Configuration	Canopy
○ BW, $R \times 10^{-6}$=0.35 to 0.49	Off
□ BW_T, $R \times 10^{-6}$=0.33 to 0.50	Off
◇ BVH, $R \times 10^{-6}$=1.33 to 1.52	Off
△ $B_TV_TH_T$, $R \times 10^{-6}$=0.73 to 0.95	Off
▽ B_TV_T, $R \times 10^{-6}$=0.73 to 0.95	Off

Theory:

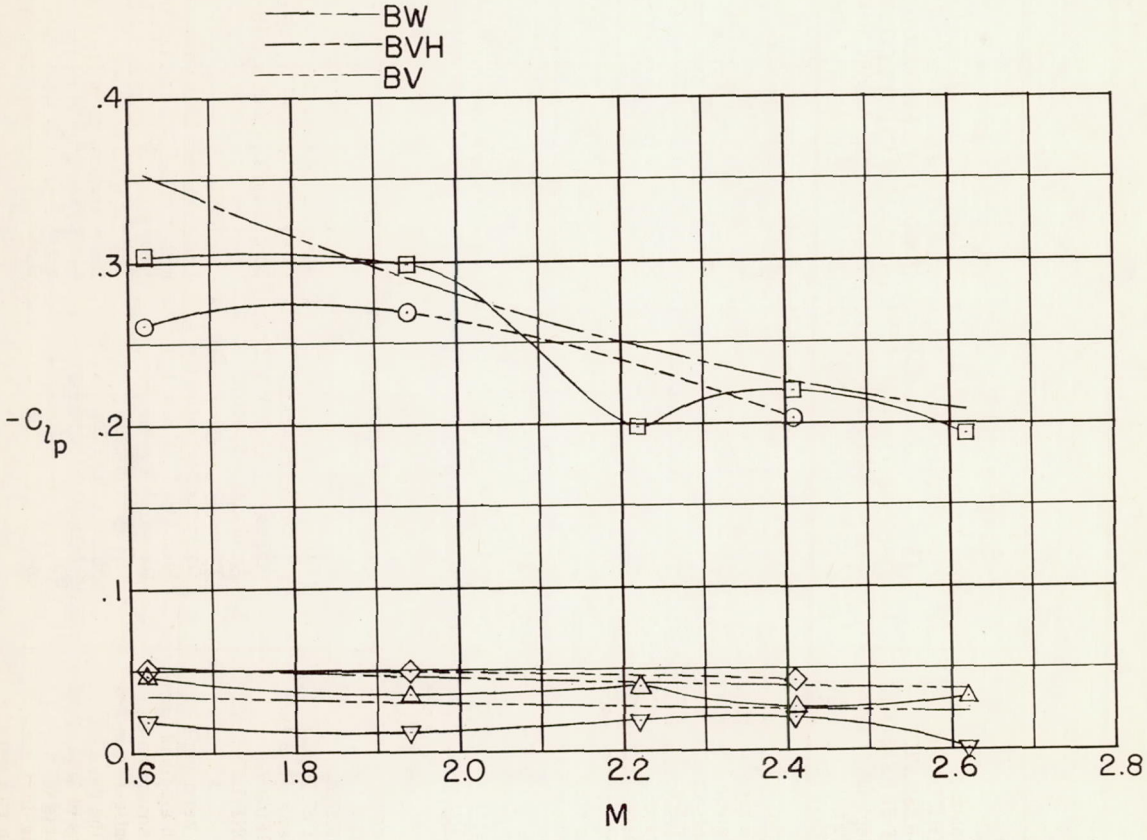

(b) $i_W = 3^\circ$.

Figure 19.- Concluded.

NACA - Langley Field, Va.